

PiC-BNN: A 128-kbit 65 nm Processing-in-CAM-Based End-to-End Binary Neural Network Accelerator

Yuval Harary*, Almog Sharoni*, Esteban Garzón[§], Marco Lanuzza[§], Adam Teman*, and Leonid Yavits*

*EnICS Labs, Faculty of Engineering, Bar Ilan University, Ramat Gan 5290002, Israel

[§] Department of Computer Engineering, Modeling, Electronics, and Systems Engineering (DIMES), University of Calabria, Rende, Italy

Email: esteban.garzon@unical.it; leonid.yavits@biu.ac.il

Abstract—Binary Neural Networks (BNNs), where weights and activations are constrained to binary values (+1, -1), are a highly efficient alternative to traditional neural networks. Unfortunately, typical BNNs, while binarizing linear layers (matrix-vector multiplication), still implement other network layers (batch normalization, softmax, output layer, and sometimes the input layer of a convolutional neural network) in full precision. This limits the area and energy benefits and requires architectural support for full precision operations. We propose PiC-BNN, a true end-to-end binary in-approximate search (Hamming distance tolerant) Content Addressable Memory based BNN accelerator. PiC-BNN is designed and manufactured in a commercial 65nm process. PiC-BNN uses Hamming distance tolerance to apply the law of large numbers to enable accurate classification without implementing full precision operations. PiC-BNN achieves baseline software accuracy (95.2%) on the MNIST dataset and 93.5% on the Hand Gesture (HG) dataset, a throughput of 560K inferences/s, and presents a power efficiency of 703M inferences/s/W when implementing a binary MLP model for MNIST/HG dataset classification.

Index Terms—Processing-in-memory, Content-Addressable Memory, Binary Neural Network, CAM, BNN, PiM.

I. INTRODUCTION

Associative, or content addressable memory (CAM), is a special type of storage that allows data access by content rather than address location. The entire contents of CAM are searched for a query and tag the position(s) where the query matches the content, exactly or approximately, e.g., within a certain Hamming distance (HD) [1], [2]. Due to their inherent parallel search capability, CAMs have been used in a variety of applications, including within the domain of artificial intelligence, where they facilitate the acceleration of neural network workloads [3]–[5].

There is a deep conceptual connection between the behavior of artificial neural networks and associative memory. In the former, the neuron with the highest correlation between the input (activation or feature) and the weight vectors points at the correct (target) class, because high correlation normally yields the highest output. In the latter, the memory row storing weights with the best (exact or most similar) match to the query (i.e., input vector) marks the target class. This effect is apparent in the case of binary neural networks (BNNs),

where both the input activations and the weights are +1 or -1, typically coded as logic ‘1’ and logic ‘0’, respectively. Therefore, the multiplication of the weights and the input feature becomes a simple XNOR operation, which is also the basic computation of associative memory.

BNNs are lightweight networks that enable very high energy efficiency by replacing full-precision multiplications by one-bit XNOR and accumulation by POPCOUNT [6]. However, in practice, multiple network components must be implemented in full precision to avoid a significant reduction in accuracy. Such components include, among others, batch normalization and biased parametric ReLU. In a convolutional BNN, the first layer is typically implemented with full precision. Furthermore, the output (fully connected) BNN layer must be implemented with high precision to be able to confidently differentiate among classes.

In summary, the requirement to implement several layers of a BNN with full precision is ubiquitous and inevitable in all types of BNNs, which makes the very definition of a BNN somewhat ambiguous. Consequently, the energy efficiency enabled by the elimination of multiplication-accumulation is significantly degraded by the need to employ auxiliary digital units or outsource full precision layers to software execution.

The purpose of this work is to implement a true *end-to-end-binary* BNN in- and using- CAM, where all network layers are binary and implemented in-memory, with no auxiliary digital processing units and without relying on software to implement full-precision calculations. We present PiC-BNN, a CAM-based classification BNN accelerator designed and fabricated in silicon using a commercial 65 nm process. We evaluate our design by implementing a binary multilayer perceptron model and measuring its classification accuracy on MNIST and Hand Gesture data sets. The PiC-BNN design achieves (close to) full baseline software accuracy on MNIST and Hand Gesture datasets and provides very high inference throughput and energy efficiency.

This work makes the following contributions:

- PiC-BNN eliminates the need for full precision operations by implementing multiple executions of the output (fully

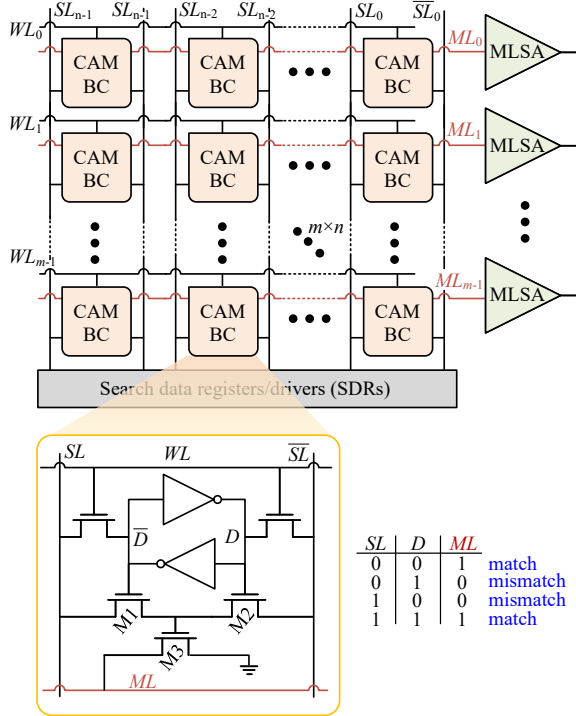


Fig. 1. Content-addressable memory (CAM). In the inset: SRAM-based NOR-type CAM cell and match and mismatch cases between searchline data SL and stored data D .

connected) layer with modified electrical parameters of CAM circuitry;

- PiC-BNN implements said modification by adjusting the approximate search-capable CAM's Hamming distance tolerance threshold rather than changing input activations or weights;
- PiC-BNN was designed and manufactured in a 65 nm commercial process and evaluated using silicon measurements.

The rest of the paper is organized as follows: Section II briefly presents the background on CAMs and BNNs. Section III presents PiC-BNN design. Section IV details the operating principle of PiC-BNN. Section V presents PiC-BNN evaluation results in terms of accuracy, performance, and power. Section VI presents the main conclusions of this work.

II. BACKGROUND

A. Content Addressable Memory

Fig. 1 shows the conventional CMOS NOR-type CAM array. The matchline (ML) is shared between bitcells of an n -bit word and also fed into a ML sense amplifier (MLSA). The searchlines (SL and \overline{SL}) are shared across all rows of the CAM array. Read and write operations within the CAM array are executed similarly to conventional six-transistor static random access memory (6T-SRAM). A CAM performs a comparison between the query data pattern that is driven onto the SLs from the search data registers (SDRs) into the

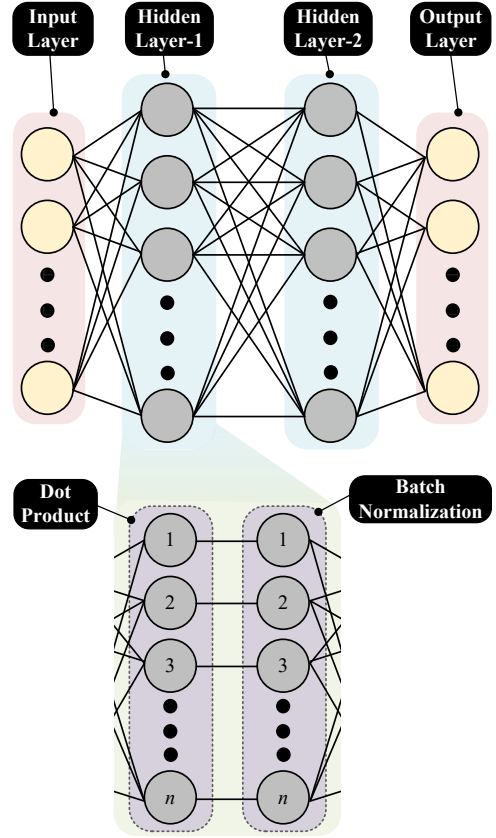


Fig. 2. Binary Neural Network: multilayer perceptron (MLP) network with two hidden layers. Each hidden layer comprises dot product (XNOR and POPCOUNT) and batch normalization layers.

memory array and the information contained within the 6T-SRAM bitcells (D and \overline{D}). This search (compare) operation is done simultaneously across the entire array during a single clock cycle in two phases: (1) ML precharge to V_{DD} ; and (2) assertion of the query data on the SLs . The MLSA evaluates the state of the ML at the end of the comparison cycle and signals a match or mismatch.

In addition to exact match CMOS-based [2] and emerging-memory-based [7]–[10] solutions, several CAM designs support approximate (including HD approximation), or similarity, search [7], [11]–[13].

B. Binary Neural Networks (BNNs)

Fig. 2 represents a class of neural networks where weights and/or activations are constrained to binary values, typically $\{-1, +1\}$. This quantization significantly reduces memory consumption and computational cost, making BNNs attractive for resource-constrained environments such as embedded systems and edge devices. By replacing full-precision arithmetic with bitwise operations, BNNs achieve efficiency while retaining an acceptable level of predictive performance for many applications [14].

In the context of multilayer perceptron (MLP) models, binarization is applied to both the weight matrices and the

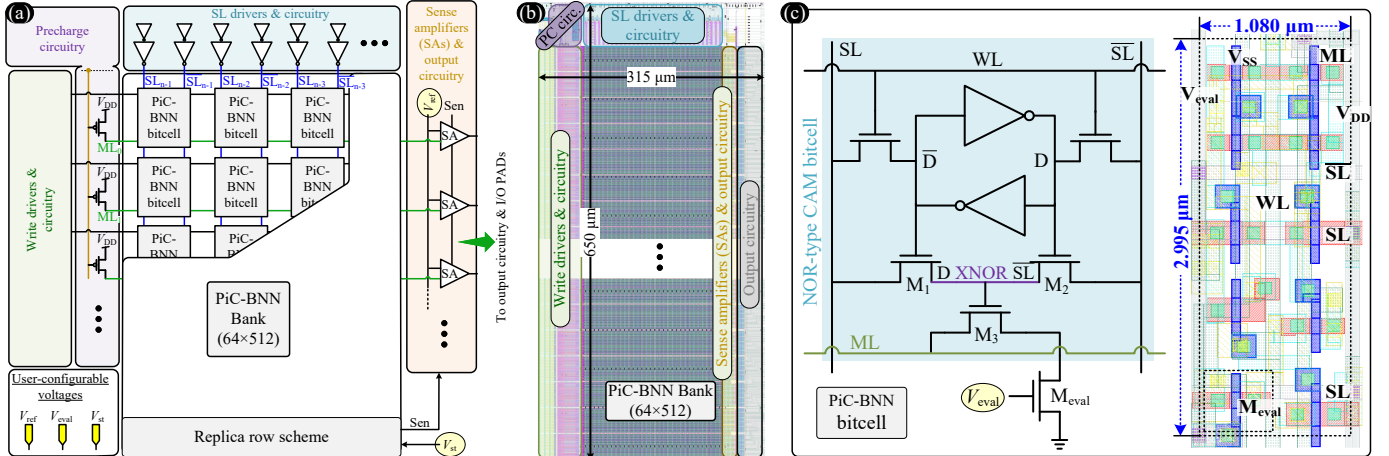


Fig. 3. (a) PiC-BNN high-level architecture of a single memory bank. (b) Layout of a 64×512 PiC-BNN bank. (c) Ten-transistor PiC-BNN bitcell and bitcell layout. Note: User-configurable voltages are highlighted in yellow in (a) and (c).

activation functions within each layer. Specifically, the forward pass in an MLP with binary weights (W) and binary activations (X) is expressed as

$$X_j^{l+1} = \phi(\text{sign}(\sum_i W_{ji} X_i^l + b^l)) \quad (1)$$

where $\text{sign}(\cdot)$ denotes the binarization function, $\phi(\cdot)$ is a non-linear activation function, X_i^l is the activation of the i -th neuron of the l -th layer, W_{ji} is the weight connecting the i -th neuron in layer l to the j -th neuron in layer $l+1$, and b^l represents the bias term in the l -th layer. Batch normalization is employed at each layer of the neural network [15]:

$$y = \sum_i (W_{ji} \cdot X_i^l), \quad (2)$$

$$X_j^{l+1} = \phi\left(\frac{y - \mu}{\sqrt{\sigma^2 + \epsilon}} \cdot \gamma + \beta\right),$$

where μ and σ are the mean and standard deviation values, and γ and β are trainable parameters. Batch normalization is essential in BNNs to achieve high accuracies, as it ensures that neuronal activations utilize both $+1$ and -1 values. At inference time, batch normalization manifests as a constant C_j in Equation (3) [16], leading to the following BNN implementation:

$$X_j^{l+1} = \text{sign}(\text{POPCOUNT}(\text{XNOR}(W_{ji}, X_i^l)) + C_j) \quad (3)$$

C. Related work: hardware BNN accelerators

Since the activations and weights of BNNs are represented by 1-bit data, neural network computations can be transformed into relatively simple XNOR and POPCOUNT operations [17]. Hardware BNN accelerators can be categorized into two main types:

- 1) Conventional digital accelerators that typically comprise XNOR gates, a POPCOUNT network, and digital accumulators to implement convolutional and fully connected binary layers [18]–[33].

- 2) Processing-in- or using-memory, often designed around resistive (memristive) memory [16], [34]–[36]. This category usually implements POPCOUNT in the analog domain and applies either Analog-to-Digital conversion (ADC) or Time-to-Digital conversion (TDC) [5], [34] in the output (fully connected) layer to preserve precision.

A separate category of BNN accelerators target CAM, employing the observation that a compare (matching) operation in a CAM row is akin to a dot-product, where per-bit matching (XNOR) emulates single-bit multiplication and the ML voltage level emulates POPCOUNT [5], [37].

A common disadvantage of TDC schemes is their high susceptibility to process, voltage, and temperature (PVT) variation [38], [39]. If a certain sampling time point is associated with a certain class, as in [34], a slight deviation from that point due to temperature or voltage drift may create a systematic error. This could result in the consistent selection of an incorrect class, making it particularly challenging to mitigate through calibration or otherwise.

The main disadvantage of ADC-based solutions is their high area and energy overhead [40] that may render the analog processing-in or using-memory implementation inefficient compared to digital or combined implementations.

III. PiC-BNN DESIGN

The PiC-BNN memory system was custom-designed in a 65 nm CMOS process, integrated within a System-on-Chip (SoC) platform, and fabricated as part of a research test chip [41]. PiC-BNN comprises four 32-kbit banks, which can be logically configured as:

- 512×256 array,
- 1024×128 array, and
- 2048×64 array.

Fig. 3(a) shows the high-level architecture of a single PiC-BNN bank, including its peripherals: SL drivers & circuitry, sensing circuitry, write circuitry, and precharge circuitry.

TABLE I
 V_{REF} , V_{EVAL} , V_{ST} COMBINATIONS AND THE HD TOLERANCE THRESHOLD LEVELS ENABLED BY THEM.

V_{ref} (mV)	V_{eval} (mV)	V_{st} (mV)	HD Tolerance
1200	1200	1200	0
750	950	1200	4
775	600	1200	8
1175	350	1150	12
950	525	1100	16
1025	475	1000	20
950	500	1025	24
775	600	1100	28
1175	400	1150	32
1000	475	725	36

Fig. 3(b) shows the layout of a single PiC-BNN bank, featuring an area footprint of about 0.21 mm^2 .

Fig. 3(c) shows the PiC-BNN bitcell, made up of a conventional 9T NOR CAM cell with an extra transistor M_{eval} in the ML discharge path to ground [1], [2]. From Fig. 3(c), the PiC-BNN bitcell layout (shown at the right) presents an area footprint of about $3.24 \mu\text{m}^2$.

To enable a wide range of HD tolerance in PiC-BNN search, we introduce three user-configurable voltage sources (highlighted in yellow in Fig. 3), as follows:

- MLSA reference voltage (V_{ref}): By lowering (raising) the V_{ref} , we increase (reduce) the HD tolerance threshold enabled by PiC-BNN.
- V_{eval} : Controls the rate of PiC-BNN ML discharge by adjusting the conductance of the M_{eval} transistor. Lowering (raising) V_{eval} slows down (speeds up) the ML discharge and thus changes the HD tolerance threshold of PiC-BNN.
- V_{st} : Adjusts the sampling time of the MLSA output. By advancing (delaying) the MLSA sampling, we increase (reduce) the HD tolerance threshold enabled by PiC-BNN.

All three user-configurable voltages are required to allow the HD tolerance to be large enough to support the required distance between the input activation and the corresponding weight vectors, as further explained in Section IV. Table I details some $(V_{\text{ref}}, V_{\text{eval}}, V_{\text{st}})$ combinations and the HD threshold levels enabled by them.

IV. OPERATING PRINCIPLE

PiC-BNN operating principle is based on two ideas presented below. The fully connected (output) layer in classification neural networks “matches” the flattened feature vector to a target class. The class that yields the highest correlation with the input feature vector is supposedly the target one. In a CAM-based fully connected layer, such correlation manifests in a “match degree”, as the closer the input vector to a class, i.e., the lower the HD between such vector and a weight vector representing the class, the higher the chance of such class to be the correct (target) one. In a BNN, the logit at the output

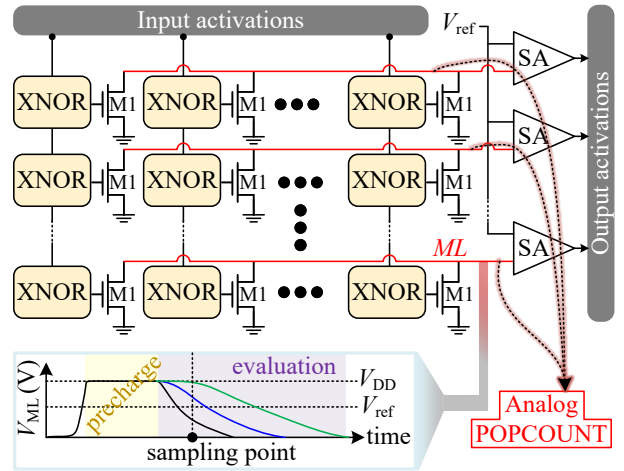


Fig. 4. PiC-BNN concept.

associated with the target class should ideally be ‘1’, while all other classes should ideally output ‘0’s. However, in real life, the target class returns ‘0’ with some probability while some of the “wrong” classes accidentally return ‘1’s. To mitigate this, prior BNN solutions implement POPCOUNT at the output of the fully connected layer at high precision by applying ADC or TDC in processing-in-memory or processing-using-memory solutions.

The law of large numbers inspires the first PiC-BNN idea: we hypothesize that if the fully connected layer is executed on the same input multiple times under different (albeit slightly) conditions, the average of the target class output will converge at ‘1’, while the averages of unrelated classes will converge at ‘0’. In other words, the majority¹ of the target class outputs across multiple passes is very likely to be ‘1’, while the majority of the outputs of any other class is very likely to be ‘0’. Such a difference in execution conditions can be achieved by modification of either the input vector or the weights of the fully connected layer in each pass. The purpose of such a modification is to create a variable HD between the input activation vector and the weights stored in the CAM rows.

Our second core idea is replacing the input or weights modification by applying approximate matching with **varying HD tolerance** threshold as a way of allowing variable HD between the input vector and the weights.

The concept of PiC-BNN is presented in Fig. 4. Logically, each PiC-BNN row performs the following operation, whose components are detailed below:

$$\mathbf{X}_j^{l+1} = \text{MAJ} \left(\sum_i \text{XNOR}(W_{ji}, \mathbf{X}_i^l) + \sum_i c_{ji} \right), \quad (4)$$

where **MAJ** is a logic majority operation, and c_{ji} are the bits of the batch normalization constant of (3) ($C_j = \sum_i c_{ji}$).

The following details the components of (4) and their implementation:

¹It could be a simple or special majority, with a threshold higher than half.

- XNOR is implemented by a per-bit matching in a PiC-BNN cell that stores a binary weight W_{ji} . The binary input activation X_i bit is asserted on SL (\bar{SL}). If $X_i \neq W_{ji}$ (representing -1), the ML discharge path through the cell opens. Otherwise, if $X_i = W_{ji}$ (representing $+1$), the ML does not discharge.
- Batch normalization parameters ($\beta, \gamma, \mu, \sigma$ of (2)) are either trainable or calculated during inference, and thereby are known in advance. Therefore, it is possible to replace batch normalization by adding to the output of a network layer (a dot product) a batch normalization constant C_j as presented in (3).

In PiC-BNN, we use the same memory to calculate the binary dot product and to add to it the batch normalization constant C_j represented as a series of $+1$ s and -1 s whose sum equals C_j . For example, $C_j = +12$ is represented by 12 matching CAM cells. Batch normalization is therefore implemented by adding a number of $+1$ s or -1 s to the $\sum_i \text{XNOR}(W_{ji}, X_i^l)$.

- Majority is implemented as follows: ML is precharged (refer to ML inset in Fig. 4) and the input activations X^l are asserted. The MLSA reference voltage V_{ref} is calibrated such that the ML voltage (V_{ML}) crosses it at the sampling time when the number of matching and mismatching bitcells in a row is the same. This way, if the number of matches exceeds the number of mismatches (refer to green line at the sampling point in Fig. 4), the ML discharges slowly and so V_{ML} crosses V_{ref} after the MLSA sampling, generating $X_i^{l+1} = 1$ (representing $+1$). Otherwise, if the number of matching cells is below the number of mismatching ones (refer to black line at the sampling point in Fig. 4), the ML discharges faster, and V_{ML} crosses the V_{ref} before the MLSA sampling time, signaling $X_i^{l+1} = 0$ (representing -1).
- To change the execution conditions of the fully connected (output) layer, we regulate the V_{ref} , adjust the pace of ML discharge by controlling V_{eval} , and set the MLSA sampling time by tuning V_{st} . Adjusting these three voltages, we induce changes in the HD between the input vector and the weights associated with a certain class, which creates a sufficient difference in each fully connected layer execution as to obtain slightly different outputs in each such execution.

V. EVALUATION

A. Accuracy evaluation

We evaluate the accuracy of the BNN MLP implemented in PiC-BNN using:

- The MNIST dataset, with 10 image classes and an image size of $28 \times 28 = 784$.
- The Hand Gesture recognition dataset [42], with 20 classes and an image size of $64 \times 64 = 4096$.

We develop and train the following MLP models

- $784 \rightarrow 128 \rightarrow 10$
- $4096 \rightarrow 128 \rightarrow 20$

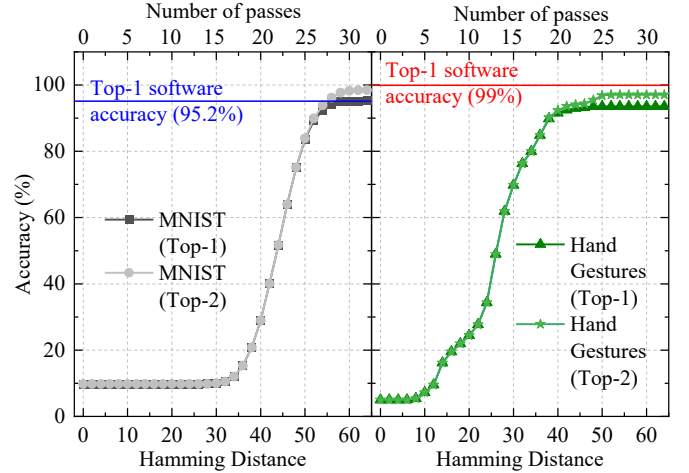


Fig. 5. TOP-1 and TOP-2 accuracy results for MNIST and Hand Gesture datasets. Note: X-axes are the number of fully connected (output) layer executions and corresponding HD tolerance threshold levels, located at the top and bottom axes, respectively.

To evaluate PiC-BNN classification accuracy, we conduct the following experiment (Algorithm 1):

Algorithm 1 Inference procedure with variable HD tolerance

```

1: for each image in each test dataset do
2:   Execute input layer: 784 (4096)  $\rightarrow$  128
3:   for HD threshold  $\in \{0, 2, 4, \dots, 64\}$  do
4:     Execute output layer: 128  $\rightarrow$  10 (20)
5:     Log the output
6:   end for
7:   Determine final prediction by majority vote in each
   class over the 33 individual outputs
8: end for

```

Accuracy evaluation results are presented in Fig. 5. The accuracy grows with the number of output $128 \rightarrow 10$ (20) layer executions and correspondingly growing HD tolerance threshold. Therefore, the PiC-BNN accuracy reaches the baseline software accuracy for MNIST (Top-1 95.2%) and Top-1 accuracy of 93.5% for Hand Gesture (vs. software baseline accuracy of 99%).

B. Performance, power consumption, and silicon area

We use silicon measurements to evaluate the performance, area, and power consumption of PiC-BNN. Fig. 6(a) presents the system-on-chip (SoC) micrograph with PiC-BNN marked. Fig. 6(b) depicts the PiC-BNN evaluation setup with its test (evaluation) board.

PiC-BNN was evaluated at 25 MHz, processing binary fully connected layers of up to 64×2048 , 128×1024 , or 256×512 (depending on CAM banks configuration) per clock cycle. Since tuning voltage sources is not an immediate operation, we apply batching to amortize tuning time across the processing of multiple images. Specifically, the same $\{V_{\text{ref}}, V_{\text{eval}}, V_{\text{st}}\}$ combination is applied to executing the fully connected (output) layer of multiple images before re-tuning it.

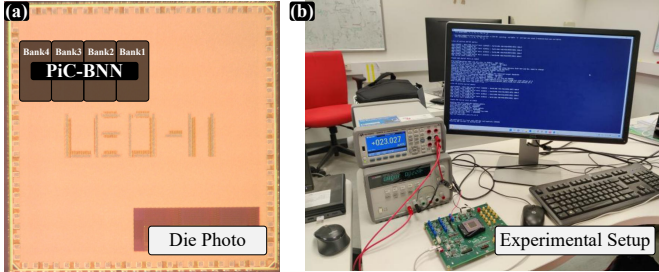


Fig. 6. (a) Die photo showing PiC-BNN as a part of a research SoC “LEO-II”. (b) Evaluation setup including the PiC-BNN PCB and a workstation.

TABLE II
SUMMARY OF PiC-BNN HARDWARE PARAMETERS.

Technology	65 nm CMOS
Supply Voltage	1.2 V
SoC Area	2.38 mm ²
PiC-BNN capacity	128 kbit
PiC-BNN area	0.87 mm ²
PiC-BNN power consumption	0.8 mW
PiC-BNN energy efficiency	184 TOPs/s
Operating Frequency	25 MHz

PiC-BNN achieves inference throughput of 560K inferences/s when implementing the $784 \rightarrow 128 \rightarrow 10$ model trained for the MNIST dataset with 33 output (fully connected) layer execution repetitions. The power consumption of PiC-BNN is 0.8 mW (at 25 °C), therefore the effective energy efficiency of PiC-BNN is about 703M inferences/s/W, or up to 184 TOPs/s without outsourcing of different BNN components to auxiliary digital processing units or software.

The overall power consumption of PiC-BNN and a RISC-V CPU that controls the SoC is about 0.3 mW. PiC-BNN silicon area is 0.87 mm². The overall SoC area (PiC-BNN and RISC-V CPU) is 2.38 mm². The performance, power consumption, and silicon area figures are summarized in Table II.

VI. CONCLUSION

In this work, we presented PiC-BNN, an in-CAM binary neural network accelerator. PiC-BNN implements a true end-to-end binary neural network, replacing full precision operations, typically outsourced to host CPU or auxiliary digital units in state-of-the-art BNN solutions, by multiple executions of the output (fully connected) layer of a classification neural network. To ensure the results of such multiple executions differ for each run, PiC-BNN uses user-configurable voltages to adjust the Hamming distance tolerance threshold of approximate matching in its CAM arrays. PiC-BNN is designed and fabricated in a commercial 65 nm process, and evaluated (classification accuracy, performance, and power consumption) using silicon measurements.

ACKNOWLEDGEMENTS

This work was supported by the Sweden-Israel Lise Meitner research collaboration under grant number 1001569396, by

the Israeli Ministry of Science, Innovation and Technology, under grants number 1001818838 and 1001702600, by the Pazy Foundation under grant number 5100089682, and by the Italian Ministry of University and Research (MUR) under grant number SOE 20240000022.

REFERENCES

- [1] E. Garzón, E. Rechef, R. Golman, O. Harel, Y. Harary, P. Snapir, M. Lanuzza, A. Teman, and L. Yavits, “A 128-kbit Approximate Search-Capable Content-Addressable Memory (CAM) With Tunable Hamming Distance,” *IEEE Journal of Solid-State Circuits*, 2025.
- [2] K. Pagiamtzis and A. Sheikholeslami, “Content-addressable memory (CAM) circuits and architectures: a tutorial and survey,” *IEEE J. of Solid-State Circuits*, vol. 41, no. 3, pp. 712–727, 2006.
- [3] A. F. Laguna, M. M. Sharifi, A. Kazemi, X. Yin, M. Niemier, and X. S. Hu, “Hardware-software co-design of an in-memory transformer network accelerator,” *Frontiers in Electronics*, vol. 3, p. 847069, 2022.
- [4] Y. Halawani, B. Mohammad, M. A. Lebdeh, M. Al-Qutayri, and S. F. Al-Sarawi, “ReRAM-based in-memory computing for search engine and neural network applications,” *IEEE Journal on Emerging and Selected Topics in Circuits and Systems*, vol. 9, no. 2, pp. 388–397, 2019.
- [5] W. Choi, K. Jeong, K. Choi, K. Lee, and J. Park, “Content addressable memory based binarized neural network accelerator using time-domain signal processing,” in *Proceedings of the 55th Annual Design Automation Conference*, 2018, pp. 1–6.
- [6] M. Zahedi, T. Shahroodi, C. Escuin, G. Gaydadjiev, S. Wong, and S. Hamdioui, “BCIM: Efficient implementation of binary neural network based on computation in memory,” *IEEE Transactions on Emerging Topics in Computing*, 2024.
- [7] A. Shaban, T.-H. Hou, and M. Suri, “SOT-MRAM-based approximate content addressable memory for DNA classification,” *IEEE Transactions on Electron Devices*, 2024.
- [8] E. Garzón, A. Bedoya, M. Lanuzza, and L. Yavits, “Monolithic 3D-Based Non-Volatile Associative Processor For High-Performance Energy-Efficient Computations,” *IEEE Journal on Exploratory Solid-State Computational Devices and Circuits (JXCD)*, vol. 10, pp. 40–48, 2024.
- [9] Y. Pan, A. Wheeldon, M. Mughal, S. Agwa, T. Prodromakis, and A. Serb, “An energy-efficient capacitive-ram content addressable memory,” *IEEE Transactions on Circuits and Systems I: Regular Papers*, 2024.
- [10] W. Xu, J. Luo, Z. Chen, B. Fu, Z. Fu, K. Wang, Q. Huang, and R. Huang, “A Novel Ferroelectric FET based Universal Content Addressable Memory with Reconfigurability for Area-and Energy-Efficient In-Memory Searching System,” *IEEE Electron Device Letters*, 2024.
- [11] C. Ni, S. Chen, C.-K. Liu, L. Liu, M. Imani, T. Kämpfe, K. Ni, M. Niemier, X. S. Hu, C. Zhuo *et al.*, “TAP-CAM: A Tunable Approximate Matching Engine based on Ferroelectric Content Addressable Memory,” in *Proceedings of the 43rd IEEE/ACM International Conference on Computer-Aided Design*, 2024, pp. 1–9.
- [12] M. M. Taha and C. Teuscher, “Approximate memristive in-memory Hamming distance circuit,” *ACM J. on Emerging Technologies in Computing Systems (JETC)*, vol. 16, no. 2, pp. 1–14, 2020.
- [13] M. Imani, A. Rahimi, D. Kong, T. Rosing, and J. M. Rabaey, “Exploring hyperdimensional associative memory,” in *2017 IEEE Int'l. Symp. on High Perf. Comp. Arch. (HPCA)*. IEEE, 2017, pp. 445–456.
- [14] C. Yuan and S. S. Agaian, “A comprehensive review of binary neural network,” *Artificial Intelligence Review*, vol. 56, no. 11, pp. 12949–13013, 2023.
- [15] S. Ioffe and C. Szegedy, “Batch normalization: Accelerating deep network training by reducing internal covariate shift,” in *Proceedings of the 32nd International Conference on Machine Learning*, F. Bach and D. Blei, Eds., vol. 37. Lille, France: PMLR, 07–09 Jul 2015, pp. 448–456.
- [16] T. Hirtzlin, M. Bocquet, B. Penkovsky, J.-O. Klein, E. Nowak, E. Vianello, J.-M. Portal, and D. Querlioz, “Digital biologically plausible implementation of binarized neural networks with differential hafnium oxide resistive memory arrays,” *Frontiers in neuroscience*, vol. 13, p. 1383, 2020.
- [17] M. Rastegari, V. Ordonez, J. Redmon, and A. Farhadi, “XNOR-Net: ImageNet classification using binary convolutional neural networks,” in *European conference on computer vision*. Springer, 2016, pp. 525–542.

[18] F. Conti, P. D. Schiavone, and L. Benini, “XNOR neural engine: A hardware accelerator IP for 21.6-fJ/op binary neural network inference,” *IEEE Transactions on Computer-Aided Design of Integrated Circuits and Systems*, vol. 37, no. 11, pp. 2940–2951, 2018.

[19] A. Al Bahou, G. Karunaratne, R. Andri, L. Cavigelli, and L. Benini, “XNORBIN: A 95 TOp/s/W hardware accelerator for binary convolutional neural networks,” in *2018 IEEE Symposium in Low-Power and High-Speed Chips (COOL CHIPS)*. IEEE, 2018, pp. 1–3.

[20] E. Nurvitadhi, D. Sheffield, J. Sim, A. Mishra, G. Venkatesh, and D. Marr, “Accelerating binarized neural networks: Comparison of FPGA, CPU, GPU, and ASIC,” in *2016 International Conference on Field-Programmable Technology (FPT)*. IEEE, 2016, pp. 77–84.

[21] G. Li, M. Zhang, Q. Zhang, and Z. Lin, “Efficient binary 3D convolutional neural network and hardware accelerator,” *Journal of Real-Time Image Processing*, vol. 19, no. 1, pp. 61–71, 2022.

[22] Q. H. Vo, N. L. Le, F. Asim, L.-W. Kim, and C. S. Hong, “A deep learning accelerator based on a streaming architecture for binary neural networks,” *IEEE Access*, vol. 10, pp. 21 141–21 159, 2022.

[23] S. Ryu, Y. Oh, and J.-J. Kim, “Binaryware: A High-Performance Digital Hardware Accelerator for Binary Neural Networks,” *IEEE Transactions on Very Large Scale Integration (VLSI) Systems*, 2023.

[24] M. Hosseini and T. Mohsenin, “Binary precision neural network many-core accelerator,” *ACM Journal on Emerging Technologies in Computing Systems (JETC)*, vol. 17, no. 2, pp. 1–27, 2021.

[25] Y. Umuroglu, N. J. Fraser, G. Gambardella, M. Blott, P. Leong, M. Jahre, and K. Vissers, “FINN: A framework for fast, scalable binarized neural network inference,” in *Proceedings of the 2017 ACM/SIGDA international symposium on field-programmable gate arrays*, 2017, pp. 65–74.

[26] R. Zhao, W. Song, W. Zhang, T. Xing, J.-H. Lin, M. Srivastava, R. Gupta, and Z. Zhang, “Accelerating binarized convolutional neural networks with software-programmable FPGAs,” in *Proceedings of the 2017 ACM/SIGDA international symposium on field-programmable gate arrays*, 2017, pp. 15–24.

[27] M. Ghasemzadeh, M. Samragh, and F. Koushanfar, “ReBNet: Residual binarized neural network,” in *2018 IEEE 26th annual international symposium on field-programmable custom computing machines (FCCM)*. IEEE, 2018, pp. 57–64.

[28] Z. Liu, B. Wu, W. Luo, X. Yang, W. Liu, and K.-T. Cheng, “Bi-real net: Enhancing the performance of 1-bit cnns with improved representational capability and advanced training algorithm,” in *Proceedings of the European conference on computer vision (ECCV)*, 2018, pp. 722–737.

[29] Z. Liu, Z. Shen, M. Savvides, and K.-T. Cheng, “Reactnet: Towards precise binary neural network with generalized activation functions,” in *Computer Vision–ECCV 2020: 16th European Conference, Glasgow, UK, August 23–28, 2020, Proceedings, Part XIV 16*. Springer, 2020, pp. 143–159.

[30] P. C. Knag, G. K. Chen, H. E. Sumbul, R. Kumar, S. K. Hsu, A. Agarwal, M. Kar, S. Kim, M. A. Anders, H. Kaul *et al.*, “A 617-TOPS/W all-digital binary neural network accelerator in 10-nm FinFET CMOS,” *IEEE journal of solid-state circuits*, vol. 56, no. 4, pp. 1082–1092, 2020.

[31] G. Qiao, S. Hu, T. Chen, L. Rong, N. Ning, Q. Yu, and Y. Liu, “STBNN: Hardware-friendly spatio-temporal binary neural network with high pattern recognition accuracy,” *Neurocomputing*, vol. 409, pp. 351–360, 2020.

[32] J. Ngadiuba, V. Loncar, M. Pierini, S. Summers, G. Di Guglielmo, J. Duarte, P. Harris, D. Rankin, S. Jindariani, M. Liu *et al.*, “Compressing deep neural networks on FPGAs to binary and ternary precision with hls4ml,” *Machine Learning: Science and Technology*, vol. 2, no. 1, p. 015001, 2020.

[33] H. Peng, S. Zhou, S. Weitze, J. Li, S. Islam, T. Geng, A. Li, W. Zhang, M. Song, M. Xie *et al.*, “Binary complex neural network acceleration on FPGA,” in *2021 IEEE 32nd International Conference on Application-specific Systems, Architectures and Processors (ASAP)*. IEEE, 2021, pp. 85–92.

[34] S. Jung, H. Lee, S. Myung, H. Kim, S. K. Yoon, S.-W. Kwon, Y. Ju, M. Kim, W. Yi, S. Han *et al.*, “A crossbar array of magnetoresistive memory devices for in-memory computing,” *Nature*, vol. 601, no. 7892, pp. 211–216, 2022.

[35] A. Azamat, F. Asim, J. Kim, and J. Lee, “Partial Sum Quantization for Reducing ADC Size in ReRAM-Based Neural Network Accelerators,” *IEEE Transactions on Computer-Aided Design of Integrated Circuits and Systems*, 2023.

[36] A. El Arrassi, M. A. Yaldagard, X. Tao, T. Shahroodi, F. Mir, Y. Biyani, M. D. Gomony, A. Gebregiorgis, R. Joshi, and S. Hamdioui, “AFSRAM-CIM: Adder Free SRAM-Based Digital Computation-in-Memory for BNN,” in *2024 IFIP/IEEE 32nd International Conference on Very Large Scale Integration (VLSI-SoC)*. IEEE, 2024, pp. 1–6.

[37] S. Choi, Y. Jeon, and Y. Seo, “High-performance and robust binarized neural network accelerator based on modified content-addressable memory,” *Electronics*, vol. 11, no. 17, p. 2780, 2022.

[38] E. Garzón, R. Golman, Z. Jahshan, R. Hanhan, N. Vinshtok-Melnik, M. Lanuzza, A. Teman, and L. Yavits, “Hamming Distance Tolerant Content-Addressable Memory (HD-CAM) for Approximate Matching Applications,” *IEEE Access*, vol. 10, pp. 28 080–28 093, 2022.

[39] E. Garzón, R. Golman, M. Lanuzza, A. Teman, and L. Yavits, “A Low-Complexity Sensing Scheme for Approximate Matching Content-Addressable Memory,” *IEEE Transactions on Circuits and Systems II: Express Briefs*, vol. 70, no. 10, pp. 3867–3871, 2023.

[40] A. Shafiee, A. Nag, N. Muralimanohar, R. Balasubramonian, J. P. Strachan, M. Hu, R. S. Williams, and V. Srikumar, “ISAAC: A convolutional neural network accelerator with in-situ analog arithmetic in crossbars,” *ACM SIGARCH Computer Architecture News*, vol. 44, no. 3, pp. 14–26, 2016.

[41] E. Garzón, R. Golman, O. Harel, T. Noy, Y. Kra, A. Pollock, S. Yuzhaninov, Y. Shoshan, Y. Rudin, Y. Weitzman, M. Lanuzza, and A. Teman, “A RISC-V-based research platform for rapid design cycle,” in *2022 IEEE International Symposium on Circuits and Systems (ISCAS)*. IEEE, 2022, pp. 2614–2615.

[42] R. Arya, “Hand gesture recognition dataset,” <https://www.kaggle.com/datasets/aryarishabh/hand-gesture-recognition-dataset>, 2021, accessed: 2025-04-10.